Laser-induced plasmas from the ablation of metallic targets: The problem of the onset temperature, and insights on the expansion dynamics

Davide Bleiner[a] and Annemie Bogaerts
Department of Chemistry, University of Antwerpen, Universiteitsplein 1, Antwerp, 2610 Flanders, Belgium

Fabio Belloni and Vincenzo Nassisi
Department of Physics, University of Lecce, via Arnesano, CP 193, 73100 Lecce, Italy

(Received 2 January 2007; accepted 1 February 2007; published online 16 April 2007)

Laser-induced plasmas are transient systems rapidly aging in few nanoseconds of evolution. Time-of-flight spectrometry allowed studying initial plasma characteristics based on frozen translational degrees of freedom, hence overcoming intrinsic limitations of optical spectroscopy. Experimental ion velocity distributions were reconstructed as developed during the longitudinal plasma expansion. The obtained onset plasma temperatures are in the range of ~18–45 eV depending on the ablated metals. Also the ion angular spreads were found to be a function of ablated metal, e.g., the narrowest for Fe, the broadest for Al, due to different collisional coupling in the plasma population. © *2007 American Institute of Physics*. [DOI: 10.1063/1.2721410]

I. INTRODUCTION

The use of pulsed laser beams to process or analyze target materials has been demonstrated in many publications to be rapid and efficient.[1–3] The characteristics of the laser-induced plasmas (LIPs) can be extremely variable in space and time, which makes LIP diagnostics[4] a complex task. The problem of identifying *onset* temperature values of the LIP is important for the experimental characterization as well as for obtaining reliable initial conditions of the LIP expansion to plug into numerical simulation codes.

The use of passive *optical spectroscopy* for LIP studies is relatively popular, though some intrinsic flaws in the temporal and the spatial scale should be pointed out. *Temporally*, optical spectroscopy does not allow accessing the LIP at times shorter than a tenth of a microsecond due to the strong continuum emission that covers all (transient) characteristic lines. *Spatially*, the measurement is merely based on the photons escaping from the so-called *radiating layer*, i.e., a cooler region near the boundary of the plasma, whereas the core photons are potentially self-absorbed.[5] Moreover, the temperature measurement is here based on the information provided by the *internal degrees of freedom* (i.e., the Rydberg states), which are not in a steady state condition, especially in the early stage of the LIP evolution.

Time-of-flight (TOF) spectrometry offers several advantages for LIP investigations,[6–11] namely, it is a noninvasive technique and allows studying LIP characteristics in an angle-resolved way [two-dimensional (2D) distributions]. Besides, it probes the pristine LIP conditions even over a long temporal range, because the measurement is based on the *translational degrees of freedom* (i.e., the ion kinetic energy), which are indeed frozen beyond the region of translational instability, the so-called *Knudsen layer* (KL). The KL forms near the surface if there are a few (three to five) collisions per particle occurring.[12] Raw TOF signals are shown in Fig. 1 for the four metals studied in this work and for three selected angles off normal, as explained below in the experimental section.

The obtained velocity distributions (Fig. 2) follow a so-called *shifted Maxwell-Boltzmann* curve, because the thermal velocity spread is superposed to a drift flow component of the center of mass. The LIP *drift velocity* must be related to the shifted peak position of the distribution, whereas the distribution spread (or Gaussian variance s^2) is proportional to the LIP kinetic temperature. The distribution function has a general form of a Gaussian as follows:

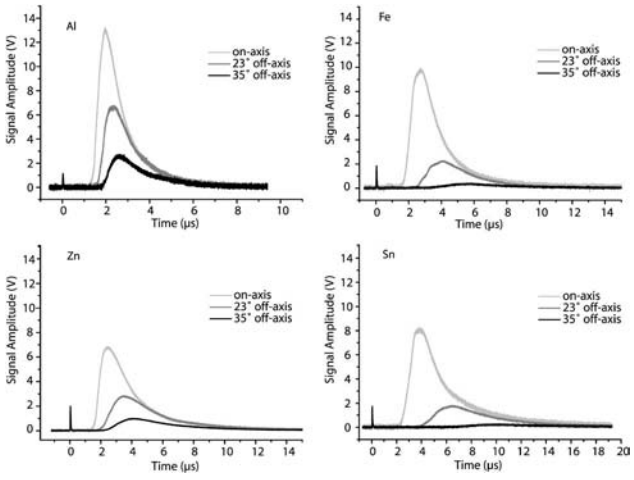

FIG. 1. Raw time-of-flight signals acquired for Al, Fe, Zn, and Sn as a function of collection angle. The time scale is triggered by the occurrence of the *photopeak*, shown at $t=0$.

[a]Author to whom correspondence should be addressed; visiting scientist at the Istituto Nazionale di Fisica Nucleare (INFN), via Arnesano CP 123, 73100 Lecce, Italy; electronic mail: davide.bleiner@ua.ac.be

$$I(\boldsymbol{v};\boldsymbol{v}_d,s^2)=\left(\frac{1}{2\pi s^2}\right)^{3/2}\exp\left[-\frac{(\boldsymbol{v}-\boldsymbol{v}_d)^2}{2s^2}\right]$$
$$=\left(\frac{m}{2\pi k_B T}\right)^{3/2}\exp\left[-\frac{m((v_z-v_d)^2+v_x^2+v_y^2)}{2k_B T}\right], \quad (1)$$

where the *variable* $\boldsymbol{v}$ is the particle velocity, and the *parameters* are the plasma drift velocity $\boldsymbol{v}_d$ (which is along the *expansion* axis z) and the distribution spread s [half-width at half maximum HWHM]. The second part of Eq. (1) shows explicitly the physical meaning of the distribution, with T the temperature at the KL upper boundary, m the ion mass, and k_B the Boltzmann constant. Henceforth, one can obtain the sought after temperature from the Maxwell-Boltzmann curve spread for a given ion as follows:

$$T=\frac{m}{k_B}s^2. \quad (2)$$

Hence, the hotter the LIP, the broader the velocity distribution for a given atom, regardless the peak position. The latter is a function of bulk flow drift velocity, and can be related to the extent of ion acceleration driven by the beam irradiation. This is influenced by the thermo-optical characteristics of the irradiated target; i.e., for constant irradiance a low boiling point material demands less energy for the phase change, so that the excess energy is used for ion thrusting.

The aim of this work was to investigate experimentally the 2D expansion and the *elliptical* temperatures[8] of several LIPs produced during the ablation of metallic samples.

II. EXPERIMENT

The ablation experiments were done using a KrF^* excimer laser (Lambda Physik, Compex) at 248 nm with a pulse duration of 23 ns, focused into a spot of approximately 1 mm^2 using a 150 mm focal length lens, resulting in an irradiance of 1.3 GW/cm^2 (Gentec joulemeter). The laser was directed to the target material with an angle of 70° off normal in order to minimize the LIP-beam interaction. The sample was located within an expansion chamber at a pressure of 3.5 mPa, which allowed LIP unperturbed expansion, since the mean free path inside the chamber was 1.8 m, i.e., much larger than the overall LIP expansion length (70 mm). The detector was a Faraday cup with a grounded circular front mask, with an array of 13 orifices along the diameter. The orifices (4 mm inside diameter) were opened alternatively to allow ion detection along a specific off-axis direction. Targets of Al, Fe, Zn, and Sn were ablated using commercially available high purity thin foils (Goodfellow Ltd., Cambridge) as samples.

III. RESULTS

A. Ion velocity distributions

Figure 2 shows the experimentally obtained ion velocity distributions from the raw TOF signals of Fig. 1 at three different collecting angles, i.e., for $\theta=0°$ (on axis) together with 23° and 35° off axis. This permits the evaluation of the angular distribution of the ion flux. The curves of Al (Fig. 2, top left), especially the off-axis ones, have a negative tailing that increases at larger collection angle. This suggests that the vast majority of fast particles are ejected within a small solid angle from the normal and thus their abundance decreases along oblique directions. This is also indicated by a series of further considerations. Firstly, the integrals of the 23° and the 35° Al curves are factors of 3 and 7 lower than that of the on-axis curve, respectively. This quantifies the absolute ion flux reduction along the oblique directions. Secondly, for the two off-axis distributions the maximum velocity is as high as 45 km/s (*cut-off value*), whereas the fast particles detected on axis (i.e., as fast as 55 km/s) are not present. This indicates a reduction of speed range along the oblique directions. The curves of Fe (Fig. 2, top right) suggest that this element is ablated with a much higher directionality than the case of Al. In fact, the integrals for the off-axis curves are much lower than the on-axis one: a factor of 10 lower for the 23° off-axis curve and a factor of 60 lower for the 35° off-axis one. Besides, if one observes the highest velocity of the three distributions, the cut-off value is at 30 km/s for the off-axis distributions, which is 15 km/s lower than the highest on-axis speed (i.e., 45 km/s). The curves of Zn (Fig. 2, bottom left) are characterized by a good symmetry and relatively large width, which suggests a high LIP temperature (Table I). The change of integral from on axis to off axis is not as dramatic as in the case of Fe (here factors of 5 and 17 for 23° and 35°, respectively), which suggests a bit more divergent particle ejection. To the curves of Sn (Fig. 2, bottom right) apply qualitatively similar considerations like in the case of Fe, i.e., high forward peaking of the plasma bunch (here factors of 16 and 30 000 for 23° and 35°, respectively), yet the ion yield is significantly lower than all other previous cases. Some of the curves are characterized by little shoulders, more pronounced off axis, which might be due to the presence of multiply charged ions in the ablated ion ensemble. Strategies of signal deconvolution were discussed and implemented elsewhere to extract the

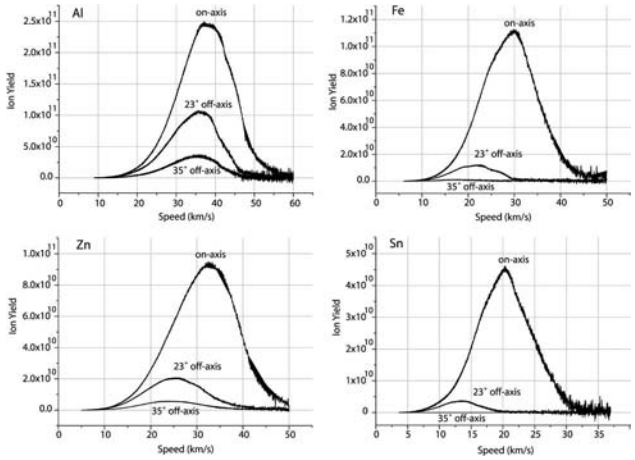

FIG. 2. Experimental velocity distribution functions for Al, Fe, Zn, and Sn ions for three different collection angles. The peak of the on-axis distribution relates to the bulk flow drift velocity, whereas the spread provides information on the LIP temperature. The curve characteristics are summarized in Table I.

TABLE I. Curve metrics of the velocity distributions shown in Fig. 2, together with calculated temperatures in eV. It should be reminded that 1 eV=kT for T=11 600 K. The degrees in the parentheses refer to the collection angle. The integrals give the total number density of ions ablated, the peak height is the maximum density, the peak position is the plasma mode velocity that on axis is the center-of-mass drift velocity, and the spread is proportional to the temperature as in Eq. (2). The LIP temperature is calculated from the on-axis spread value. N/A is "not available," because the profile was not well above background level.

Target	Integral $f(v)dv$ ($m^{-2}\,s^{-1}$)	Peak height $f_{max}(v)$ (m^{-3})	Peak position (km/s)	FWHM spread (km/s)	LIP energy (eV)
Al	4.3×10^{15} (0°)	2.5×10^{11} (0°)	37.1 (0°)	16.0 (0°)	18.5±0.3
	1.5×10^{15} (23°)	1.1×10^{11} (23°)	35.5 (35°)	15.0 (23°)	
	6.2×10^{14} (35°)	3.7×10^{10} (35°)	35.6 (23°)	14.0 (35°);	
Fe	1.6×10^{15} (0°)	1.1×10^{11} (0°)	29.8 (0°)	14.0 (0°)	27.0±0.4
	1.5×10^{14} (23°)	1.2×10^{10} (23°)	22.6 (23°)	11.0 (23°)	
	2.5×10^{13} (35°)	N/A (35°)	N/A (35°)	N/A (35°)	
Zn	1.6×10^{15} (0°)	9.5×10^{10} (0°)	32.5 (0°)	16.0 (0°)	44.3±0.7
	3.3×10^{14} (23°)	2.1×10^{10} (23°)	26.3 (23°)	15.0 (23°)	
	9.6×10^{13} (35°)	5.8×10^{9} (35°)	23.6 (35°)	15.0 (35°)	
Sn	4.7×10^{14} (0°)	4.6×10^{10} (0°)	20.4 (0°)	9.8 (0°)	29.5±0.4
	2.9×10^{13} (23°)	3.8×10^{9} (23°)	13.3 (23°)	6.9 (23°)	
	1.6×10^{10} (35°)	1.1×10^{7} (35°)	N/A (35°)	N/A (35°)	

charge state distributions.[13] The obtained LIP temperatures for the four metals, together with the LIP drift velocities, as deduced from the measured Maxwell-Boltzmann curves, are summarized in Table I.

B. Ion angular distributions

Hence, as a rule, these experiments indicate that ablated ions are highly directional and normal to the irradiated surface. Regarding such LIP forward peaking (or angular spread), Fig. 3 shows the integrated signals as a function of collection angle. The forward peaking of the ion velocity distributions is obviously a function of ablated metal. Although the use of the "$\cos^p\theta$" fitting function is popular,[14] its use has mostly a heuristic validity. Hence, we derived a more stringent physical link between the profiles and the experimental conditions. Our simulated curves stem from a Lorentzian distribution function[15] that is defined as follows:

$$\mathrm{I}(\vartheta;\vartheta_c,\gamma)=\mathrm{I}_0+\frac{A}{\pi}\left(\frac{\phi}{(\vartheta-\vartheta_c)^2+\phi^2}\right), \tag{3}$$

where the variable θ is the off-axis angle, and the parameters of the distribution are θ_c, which is the location of the peak, and ϕ, which is the Γ parameter of the Lorentzian or the angular distribution's spread (HWHM). The *peak position* in Fig. 3 is not at 0° because the ablation site was offset to the ion collector center, so that we could observe a wider angle of the plume on one side. Finally, the parameter A is the integral of the distribution and I_0 is the background offset.

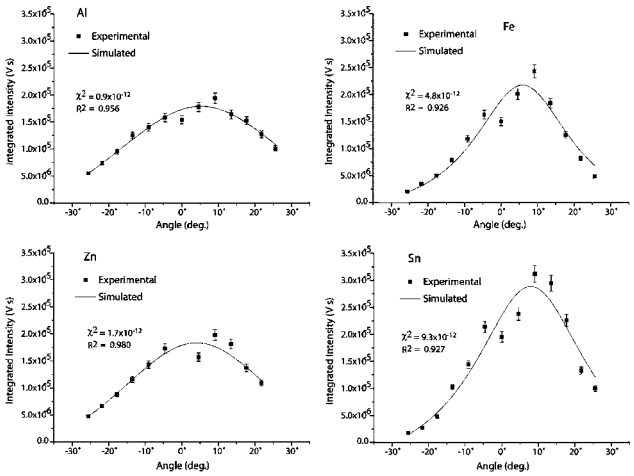

FIG. 3. Experimental angular distribution of the TOF integrated intensities for Al, Fe, Zn, Sn, and simulated profiles obtained with a Lorentz distribution. The following angular distribution values were determined: Al, 37°±11°; Fe, 16°±4°; Zn 32°±4°; and Sn 17°±4°.

The use of a Lorentzian distribution function for fitting angular distribution data is motivated by both physical and mathematical reasons. Firstly, it is well known that, given two *variates* X and Y that follow a Gaussian distribution, the distribution of their ratio, i.e., $R=X/Y$, follows the so-called *Cauchy distribution* (so-called "Lorentz distribution" in spectroscopy).[16] In our physical problem, the *transversal* (T) and the *longitudinal* (L) ion velocity components are indeed variates with Maxwell-Boltzmann (i.e., Gaussian) distribution. Their ratio defines the tangent of the spread angle, i.e., $v_T/v_L=\tan\vartheta$. For $\vartheta\leqslant40°$ one can approximate the tangent to a linear function, i.e., $\tan\vartheta\sim\vartheta$, within an accuracy of 1%. In conclusion, the *spread angle distribution* can be properly described using the Lorentz distribution.

To implement such a theory, some additional considerations are necessary on the mechanics of particle collisions in the KL. Such a treatment considers a thin layer transported longitudinally and laterally infinite, i.e., an assumption justified by the geometry of the KL, whose aspect ratio is typically small. Firstly, *head-on* collisions do not contribute to a transverse spread but simply to the forward transport. On the other hand, *offset* collisions produce a (nonzero) *net* scatter-

ing angle, only when transverse displacement is physically possible considering the packing in the KL. Otherwise, offset collisions in a packed KL produce also forward transport due to *channeling*. In fact, at the instant of collision between two particles *A* and *B*, a line drawn through the centers of such particles delimits an angle ϕ_{AB} from the longitudinal axis of forward motion. Such an angle is the angle of free emergence for the hit particle. However, the hit particle (s) might further collide with other particles, and so on. The bulk combination of particle-particle collisions determines a *statistical distribution* of collision angles, with one dominating value ϕ. A LIP forward peaking is favored by a *strong* collisional coupling (i.e., high *fluid flow viscosity*) in the KL. On the other hand, under weak collisional coupling, the individual particle paths can easily depart from the main flow direction, i.e., the LIP angular spread is enhanced (i.e., low fluid viscosity).

IV. DISCUSSION

The *collisional coupling* was expressed introducing a quantitative criterion, defined from the ratio between the cross sections of interaction and the geometric spacing among particles. For this purpose, the ion collision cross section (σ_{ion}) is normalized to the collision-free area around the particle. The *effective* Coulomb collision cross section is a function of charge state and LIP temperature and is moderated by the potential presence of electrons in the plasma, which screen out the fields. Using the *Debye length* in the LIP as the radius, one obtains such a Coulombic cross section, i.e., $\sigma_{\text{ion}}=\pi\lambda_D^2$ with the Debye length defined as $\lambda_D \equiv \sqrt{k_B T_e/4\pi e^2 n_e}$.[5] For our experiments Debye lengths in the millimeter range could be calculated, based on TOF temperatures measured in this work (see Table I) and on electron number densities obtained previously,[13] namely, λ_D for Al was 4.3 mm, for Fe was 1.3 mm, for Zn was 1.8 mm, and for Sn was 1.2 mm.

The particle-to-particle *collision offset* distance *b* (also known as *impact parameter* in the physics jargon) is used for the computation of the collision-free area. This is easily calculated from the mean free path λ considering the angle of collision, i.e., $b=\lambda \sin\phi$ Hence, we expressed the LIP collisional coupling (proportional to the fluid flow viscosity, and hence the forward peaking) as follows:

$$\rho = \frac{\pi\lambda_D^2}{\pi(\lambda \sin\phi)^2} = \left(\frac{\lambda_D/\lambda}{\sin\phi}\right)^2. \tag{4}$$

Using Eq. (4), the collisional coupling can be related to the LIP transverse spread as well as the physical characteristics. The ratio λ_D/λ is indeed the *inverse* of the Knudsen number, i.e., a large value indicates a continuum fluidlike behavior, whereas a small value suggests the behavior typical of an ensemble of discrete particles.

The threshold between fluid and particle behavior is important, and it is discussed in the following with a few considerations on the LIP dynamics. For the case of *statistically dominating* head-on collisions, one obtains that $\phi \sim 0°$ and consequently in Eq. (4) is $\rho_{\phi=0} \sim \infty$. Thus, a high ρ value indicates that the LIP forward peaking is high, as the fluid viscosity, and transverse spread of the particles is impeded by a densely packed KL. In this extreme case of $\rho=\infty$, the system expands one dimensionally with essentially a forward velocity component *L* only. On the other extreme, i.e., of just *grazing collisions*, particle collisions have a free emergence angle of $\phi \sim 90°$ that leads to $\rho_{\phi=90} \sim (\lambda_D/\lambda)^2 \equiv \rho_{\text{thr}}$. This is the *threshold* for the collisional coupling and continuum fluid behaviour ($\rho/\rho_{\text{thr}}=1$). For $\rho\rho_{\text{thr}}<1$ the ions are loose and collisions are statistically improbable [see Eq. (4a) bis below]. In such a case, the system cannot be described as a continuum fluid due to an inviscid advection, rather as an ensemble of particles with independent pathways. Hence, in general we can write the following dependence between the collisional coupling factor and the angle of LIP spread:

$$\langle \rho/\rho_{\text{thr}} \rangle = \frac{1}{\sin^2\phi}. \tag{4a}$$

The higher the ρ_{thr} term, the higher the *particle-to-fluid threshold*, and this favors the tendency of the LIP to spread laterally. The particle-to-fluid threshold is a function of LIP physical conditions, which can be expressed explicitly using the definition of the Debye length [numerator and symbols before the slash sign in Eq. (5) below] and mean free path in the KL (denominator after the slash), to obtain the following parametric dependence (i.e., besides the constants):

$$\rho_{\text{thr}} = \left(\frac{\lambda_D}{\lambda}\right)^2 = \left[\frac{k_B T}{4\pi e^2 n_e}\right] \Big/ \left[\frac{1}{(n\sigma_{\text{ato}})^2}\right] \propto n_e T \left(\frac{\sigma_{\text{ato}}}{z}\right)^2, \tag{5}$$

where *n* denotes the number density of all heavy particles, which can be combined with the electron number density in the plasma charge as $z \equiv n_e/n$ (valid considering *quasineutrality* and the absence of negative ions).[5] Equation (5) shows that the threshold increases with the electron number density (n_e), the LIP temperature (*T*), and more sensitively with the heavy particle cross section (σ_{ato}), whereas the charge *z* lowers the threshold with a power-of-2 dependence. Hence, as a general rule, the LIP angular spread is *wider*, for a low ratio $\rho\rho_{\text{thr}}$, which generally suggests that the LIP charge is weak, and the electron density and the temperature are more remarkable [see Eq. (5)].

Using Eq. (4), we calculated the following element-dependent collisional coupling numbers: $\rho_{\text{Al}}=3.0\times10^4$, $\rho_{\text{Fe}}=5.1\times10^6$, $\rho_{\text{Zn}}=2.2\times10^6$, and $\rho_{\text{Sn}}=7.5\times10^6$. These results indicate that the LIP from Al is two to three orders of magnitude looser (lower fluid viscosity) than the ones from ablation of Fe, Zn, and Sn. Hence, the lateral spread of Al is the result of the modest coupling among the individual particles, which is about a factor of 3 above the threshold for fluid behavior (i.e., for Al $\rho/\rho_{\text{thr}}=2.7$). The LIPs of Fe ($\rho/\rho_{\text{thr}}=12.5$) and Sn ($\rho/\rho_{\text{thr}}=11.7$), due to a stronger particle coupling, behave more fully as *continuum fluids*, being more than one order of magnitude above the threshold. The LIP from Zn, due to a slightly *higher* threshold value than for Fe, is characterized by a somewhat wider spread in spite of the high ρ_{Sn} (for Zn $\rho/\rho_{\text{thr}}=3.5$, i.e., close to Al). This also suggests that the higher temperature of the Zn plasma is not matched by a consistent increase of the charge, which may

be explained with the higher ionization potential of Zn versus Fe. The higher temperature of the Zn plasma might be attributed to a low boiling point of this metal, so that for Zn the laser energy exceeding the thermodynamic demand for heating and melting/boiling is larger, i.e., $\Delta E = E_{\text{laser}} - E_{\text{therm}}$, and stored in the plume.

A. The LIP temperature

In conclusion, the range of electron or ion temperatures of a LIP reported in the literature, obtained using passive spectroscopy under different operating conditions (wavelength, irradiance, etc.),[17–26] are mostly lower than 30 000 K. However, the optical spectroscopy techniques permit us to determine temperatures related to electron, atom, or ion modes on a *mid-long term* with respect to the time scale of the plume evolution, namely from approximately *tenths* up to a few *tens* microseconds. On the other hand, in Claesyssens *et al.*[27] velocity distributions comparable to ours have been obtained using a less oblique laser beam (45°), yet the extracted kinetic energies (KEs) are of ~100 eV. Similarly, in Amoruso *et al.*[28] the KE values reported are of the order of 100 eV, as obtained using a longer wavelength (355 nm) and with 30° beam delivery, which implies a slightly stronger beam-plasma interaction than in our case. Such KE values would imply dramatically high LIP temperatures of almost 10^6 K, though unfortunately the data reduction procedure has not been exposed. The present work's values are well above the optical spectroscopy values because we could measure onset temperatures related to the instant when the ions achieve translational equilibrium at the KL's *upper boundary*. We have decoupled the *thermal* component and the *drift* component in order to obtain representative temperatures (i.e., using the thermal component only). Our values are in agreement with TOF measurements reported by Franghiadakis *et al.*[6] obtained using a tenfold larger target-detector distance (~700 mm), which demonstrates that the translational degrees of freedom are frozen, as well as with own computational results.[29]

The temperature values obtained are higher than all target elements' *first ionization potential* ($IP^{I \to II}$: Al=6.0 eV, Fe=7.9 eV, Zn=9.4 eV, Sn=7.3 eV) and for some of them these values are even above the second ionization potential ($IP^{II \to III}$: Al=18.8 eV, Fe=16.2 eV, Zn=18.0 eV, Sn =14.6 eV), which suggest a fully ionized plasma. It should be remarked that since the laser beam was oblique to the target surface, the obtained temperatures must be considered as primary, i.e., negligible laser-plume interaction takes place, modifying the plasma energy balance.

V. CONCLUSIONS

This work's results would suggest a high degree of ionization for the LIP in the very early stages (plume-to-plasma *transition*), already at a modest laser beam irradiance of 1.3 GW/cm^2. Then, a rapid reduction of charge presumably occurs due to recombination (plasma-to-plume *backup*). In general, it should be noted that a rather weak LIP, both in terms of temperature and in terms of forward peaking, is associated with the ablation of Al, which confirms our previous computational results reporting on melt expulsion as the main Al ablation mechanism.[29] On the other hand, a hot and dynamic LIP is produced during the ablation of a low boiling point material such as Zn, with significant angular spread and high temperature. Extremely high temperatures might also be of technological interest for using LIP as charged particles or radiation sources in the extreme ultraviolet range.

ACKNOWLEDGMENTS

F. Grancagnolo (INFN-Lecce) is acknowledged for support. Discussions with R. Gijbels, D. Autrique, A. Lorusso, D. Doria, and L. Velardi are acknowledged.

[1] P. R. Willmott, Prog. Surf. Sci. **76**, 163 (2004).
[2] R. E. Russo, X. L. Mao, H. C. Liu, J. Gonzalez, and S. S. Mao, Talanta **57**, 425 (2002).
[3] D. Bleiner, F. Belloni, D. Doria, A. Lorusso, and V. Nassisi, J. Anal. At. Spectrom. **20**, 1337 (2005).
[4] I. H. Hutchinson, *Principles of Plasma Diagnostics* (Cambridge University Press, Cambridge, 2002).
[5] Ya. B. Zel'dovich and Yu. P. Raizer, *Physics of Shock Waves and High-Temperature Hydrodynamic Phenomena* (Dover, New York, 2002).
[6] Y. Franghiadakis, C. Fotakis, and P. Tzanetakis, Appl. Phys. A: Mater. Sci. Process. **68**, 391 (1999).
[7] J. Krasa, A. Lorusso, D. Doria, F. Belloni, V. Nassisi, and K. Rohlena, Plasma Phys. Controlled Fusion **47**, 1339 (2005).
[8] J. C. S. Kools, T. S. Baller, S. T. De Zwart, and J. Dieleman, J. Appl. Phys. **71**, 4547 (1992).
[9] K. J. Koivusaari, J. Levoska, and S. Leppävuori, J. Appl. Phys. **85**, 2915 (1999).
[10] Y. F. Lu, M. H. Hong, and T. S. Low, J. Appl. Phys. **85**, 2899 (1999).
[11] R. Kelly and R. W. Dreyfus, Nucl. Instrum. Methods Phys. Res. B **32**, 341 (1988).
[12] I. Noorbatcha, R. Lucchese, and Y. Zeiri, J. Chem. Phys. **86**, 5816 (1987).
[13] A. Picciotto, J. Krasa, L. Laska, K. Rohlena, L. Torrisi, S. Gammino, A. M. Mezzasalma, and F. Caridi, Nucl. Instrum. Methods Phys. Res. B **247**, 261 (2006).
[14] K. L. Saenger, J. Appl. Phys. **70**, 5629 (1991).
[15] R. A. Treumann, Phys. Scr. **59**, 19 (1999).
[16] E. W. Weisstein, http://mathworld.wolfram.com/CauchyDistribution.html
[17] V. S. Burakov, N. V. Tarasenko, and N. A. Savastenko, Spectrochim. Acta, Part B **56**, 961 (2001).
[18] G. Abdellatif and H. Imam, Spectrochim. Acta, Part B **57**, 1155 (2002).
[19] E. M. Monge, C. Aragon, and J. A. Aguilera, Appl. Phys. A: Mater. Sci. Process. **69**, S691 (1999).
[20] B. Le Drogoff, J. Margot, F. Vidal, S. Laville, M. Chaker, M. Sabsabi, T. W. Johnston, and O. Barthelemy, Plasma Sources Sci. Technol. **13**, 223 (2004).
[21] J. A. Aguilera, J. Bengoechea, and C. Aragon, Spectrochim. Acta, Part B **59**, 461 (2004).
[22] M. Corsi, G. Cristoforetti, M. Giuffrida, M. Hidalgo, S. Legnaioli, V. Palleschi, A. Salvetti, E. Tognoni, and C. Vallebona, Spectrochim. Acta, Part B **59**, 723 (2004).
[23] L. M. Cabalin and J. J. Laserna, Spectrochim. Acta, Part B **53**, 723 (1998).
[24] M. A. Hafez, M. A. Khedr, E. F. Elaksher, and Y. E. Gamal, Plasma Sources Sci. Technol. **12**, 185 (2003).
[25] G. W. Rieger, M. Taschuk, Y. Y. Tsui, and R. Fedosejevs, Spectrochim. Acta, Part B **58**, 497 (2003).
[26] V. Detalle, M. Sabsabi, L. St-Onge, A. Hamel, and R. Heon, Appl. Opt. **42**, 5971 (2003).
[27] F. Claeyssens, S. J. Henley, and M. N. R. Ashfold, J. Appl. Phys. **94**, 2203 (2003).
[28] S. Amoruso, Appl. Surf. Sci. **138-139**, 292 (1999).
[29] D. Bleiner, Z. Chen, D. Autrique, and A. Bogaerts, J. Anal. At. Spectrom. **21**, 910 (2006).